Editors' Suggestion

Trends in pressure-induced layer-selective half-collapsed tetragonal phases in the iron-based superconductor family $AeA\mathrm{Fe_4As_4}$

Vladislav Borisov,[1,*] Paul C. Canfield,[2,3] and Roser Valentí[1]

[1]*Institute of Theoretical Physics, Goethe University Frankfurt am Main, D-60438 Frankfurt am Main, Germany*

[2]*Ames Laboratory US DOE, Iowa State University, Ames, Iowa 50011, USA*

[3]*Department of Physics and Astronomy, Iowa State University, Ames, Iowa 50011, USA*

(Received 6 June 2018; published 24 August 2018)

By performing pressure simulations within density functional theory for the family of iron-based superconductors $AeA\mathrm{Fe_4As_4}$ with Ae = Ca, Sr, Ba and A = K, Rb, Cs we predict in these systems the appearance of two consecutive half-collapsed tetragonal transitions at pressures P_{c_1} and P_{c_2}, which have a different character in terms of their effect on the electronic structure. We find that, similar to previous studies for $\mathrm{CaKFe_4As_4}$, spin-vortex magnetic fluctuations on the Fe sublattice play a key role for an accurate structure prediction in these materials at zero pressure. We identify clear trends of critical pressures and discuss the relevance of the collapsed phases in connection to magnetism and superconductivity. Finally, the intriguing cases of $\mathrm{EuRbFe_4As_4}$ and $\mathrm{EuCsFe_4As_4}$, where Eu magnetism coexists with superconductivity, are discussed as well in the context of half-collapsed phases.

DOI: 10.1103/PhysRevB.98.064104

I. INTRODUCTION

The so-called 122 Fe-based pnictides [Fig. 1(b)] ($A\mathrm{Fe_2As_2}$, $Ae\mathrm{Fe_2As_2}$, $\mathrm{EuFe_2As_2}$) with A alkali and Ae alkaline-earth cations crystallize at room temperature in a body-centered tetragonal $\mathrm{ThCr_2Si_2}$ structure ($I4/mmm$) [1,2], where As sites from the neighboring Fe-As blocks face each other across the A or Ae plane. The As-As interlayer distance in these systems can be then tuned by either mechanical or chemical pressure down to sufficiently small values, allowing the formation of As-As p_z bonds. This is accompanied by a structural phase transition to a collapsed tetragonal (cT) phase where the c/a ratio is significantly reduced due to a dramatic contraction of the c-lattice parameter and a slight expansion of the a-lattice parameter. This process is known to suppress superconductivity or/and long-range "stripe" magnetic order [Fig. 1(d)] due to the crossover to a more three-dimensional structure and the loss of spin fluctuations and local Fe moments caused by a compression of Fe-As bonds [3]. In the 122 materials, the transition to a cT phase affects the whole structure leading to As-As p_z bond formation across each cation spacer layer.

In contrast, a *half-collapsed* tetragonal (hcT) phase transition was recently reported for the 1144 material $\mathrm{CaKFe_4As_4}$ [4] [Fig. 1(c)], where the periodic arrangement of Ca and K spacer layers produces two different kinds of As sites [5–7] and the tetragonal structure ($P4/mmm$) shows a layer-selective collapse upon application of pressure. First, at 4 GPa, the As-As p_z bonding across the Ca layer induces a cT transition with disappearance of superconductivity while a second collapsed transition across the K layer was predicted around ∼12 GPa. Furthermore, Ref. [4] showed that "hedgehog" [spin-vortex, Fig. 1(e)] magnetism had to be invoked in the pressure-dependent density functional theory (DFT) simulations to predict the observed structural transitions. This magnetic order has been recently measured upon electron-doping $\mathrm{CaKFe_4As_4}$ [8].

The rare-earth-based $\mathrm{EuRbFe_4As_4}$ and $\mathrm{EuCsFe_4As_4}$ are also attracting growing attention due to the coexistence of Eu magnetism and bulk superconductivity as reported in Refs. [10–13]. However, the exact nature of the Eu magnetic order and its effect on the superconductivity remain to be elucidated, as well as possible Eu^{2+} to Eu^{3+} transitions previously observed for 122 systems [14]. The interactions between the localized Eu spins are expected to be sensitive to the lattice parameters and, in this respect, the half-collapse transition might influence the ground state, which stimulates a detailed study.

Predicting the appearance of possible cT transitions in $\mathrm{ThCr_2Si_2}$-structured intermetallic compounds is not only of relevance for the superconducting and magnetic properties of these materials but also for their potential superelastic behavior as has been recently shown [15].

In this paper, we systematically study via DFT calculations possible pressure-induced hcT transitions in a series of previously synthesized 1144 systems [5] with the following combinations of the spacer cations: CaRb, CaCs, SrRb, SrCs, and BaCs,[1] as well as EuRb and EuCs. We discuss the tendencies expected for the transition pressures in relation to the nature of the spacer cations, the underlying Fe-moment fluctuations, and possible magnetism in Eu for the latter two systems.

*Corresponding author: borisov@itp.uni-frankfurt.de

[1]We note that the exact crystal structure of $\mathrm{BaCsFe_4As_4}$ is not completely clarified and this material can probably exist both in the 122 and in the 1144 forms due to a smaller difference in the cation radii, compared to other 1144 systems. Nevertheless, we include the 1144 phase of $\mathrm{BaCsFe_4As_4}$ in our simulations to reveal general trends in the 1144 family of iron pnictides.

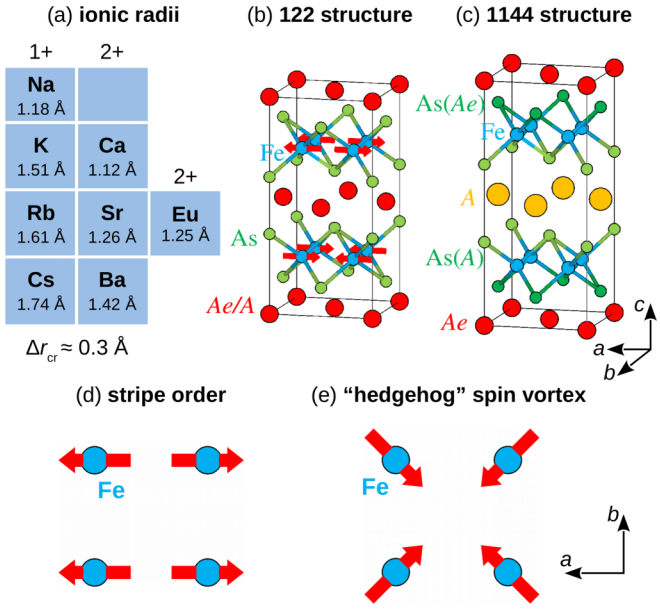

FIG. 1. (a) Cations of alkali (1+) and alkaline-earth (2+) elements, as well as divalent Eu, together with their ionic radii from Refs. [5,9]. (b) The 122 and (c) 1144 structures of iron pnictides. In general, the 1144 phase of $AeA\mathrm{Fe_4As_4}$ is stable when the difference in the ionic radii $\Delta r = |r(Ae) - r(A)|$ is larger than 0.3 Å. Possible Fe magnetic orders are shown in (d) stripe order and (e) "hedgehog" or spin-vortex order.

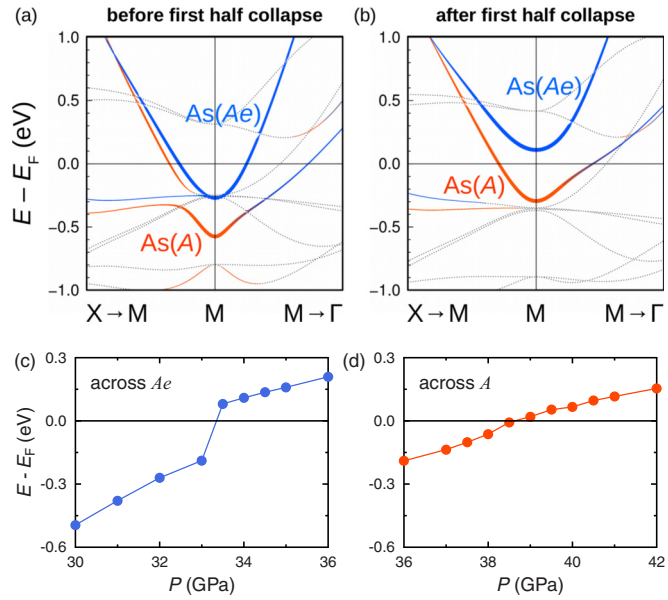

FIG. 2. (a), (b) Characteristic evolution of the non-spin-polarized band structure [31] and (c), (d) the energy position E of the antibonding As-As p_z orbital relative to the Fermi energy E_F across a hcT transition in $AeA\mathrm{Fe_4As_4}$ ($\mathrm{BaCsFe_4As_4}$ data are taken here as an example). Upon the first hcT, only the As-As p_z antibonding band from the As facing the smaller cation layer, in this case Ae (blue lines), shifts abruptly above the Fermi level (plot c), while the band from As facing the larger cation layer (orange lines) remains occupied. This suggests that As-As bonds are strongly formed across the Ae layer. The second hcT at higher pressures is identified in the same fashion and, in contrast to the first hcT, reveals a smooth shift of the corresponding As bands across the Fermi level (plot d).

II. METHODS

Structural transitions under pressure are simulated using the projector-augmented wave method [16,17] as implemented in the VASP code [18–20] within the GGA exchange-correlation approximation [21]. For the two systems with Eu, strong correlations for the *4f* states were included using two different GGA+U schemes [22,23]. Convergence of the properties of interest is achieved for a $(5 \times 5 \times 5)$ k-mesh and an energy cutoff of 600 eV. Increase of the cutoff up to 800 eV changes the c-lattice parameter by $\sim$0.05 Å and the critical pressure by less than 0.5 GPa (see Fig. 8 in Appendix B), which is an acceptable accuracy for studying the pressure-structure trends in the 1144 systems.

At low pressures, the structural prediction is done while imposing a "frozen" spin-vortex configuration of Fe moments [Fig. 1(e)], which simulates, to a first approximation, the effect of spin fluctuations, as shown in our previous work on $\mathrm{CaKFe_4As_4}$ [4,24]. The assumption of a particular underlying Fe magnetism is necessary for a correct prediction of the cT transition, even if the actual system doesn't show any long-range magnetic order. Purely nonmagnetic calculations in Fe-based superconductors fail to reproduce the correct structural parameters [25–29]. For $\mathrm{EuRbFe_4As_4}$ and $\mathrm{EuCsFe_4As_4}$, we impose the fully ferromagnetic order along the [100] direction on the Eu sublattice, in addition to the Fe spin vortex. For selected pressures, the stripelike order within each Eu layer is compared to the ferromagnetic one in terms of the enthalpy to identify possible first-order transitions related to Eu spins. Such antiferromagnetic order appears not to affect the optimized structure though.

Once the optimized 1144 structures under pressure are obtained, the electronic bands are calculated using the all-electron full-potential localized orbitals basis set (FPLO) code [30] with the GGA exchange-correlation functional (GGA+U for Eu-based systems). The critical pressure for a hcT transition is captured by monitoring the energy position of the antibonding As-As $4p_z$-based molecular orbitals, which shift towards the Fermi level with increasing pressure. At the transition, these bands shift abruptly above the Fermi level [compare Figs. 2(a) and 2(b)] and the corresponding As-As p_z bonds are enhanced. This criterium was successfully applied to several $AeFe_2As_2$ systems (Ae = Ca, Sr, Ba) [3,26–28,32,33], as well as to $\mathrm{CaKFe_4As_4}$ [4]. As shown in Figs. 2(c) and 2(d), the As band shift corresponding to the second hcT phase at higher pressures is smoother than the one corresponding to the first hcT phase.

III. RESULTS (ZERO PRESSURE)

For all systems studied here, we find that the assumption of a spin-vortex-type magnetism in our DFT calculations is crucial to reproduce the experimental structure at zero pressure as shown in Fig. 3 where the measured c- and a-lattice parameters are compared with the optimized ones. In contrast, c is severely underestimated by $\sim$(0.5–1.0) Å and a is overestimated by 2% in nonmagnetic calculations (dashed lines in Fig. 3). We note, however, that the theoretical values for the c parameter still

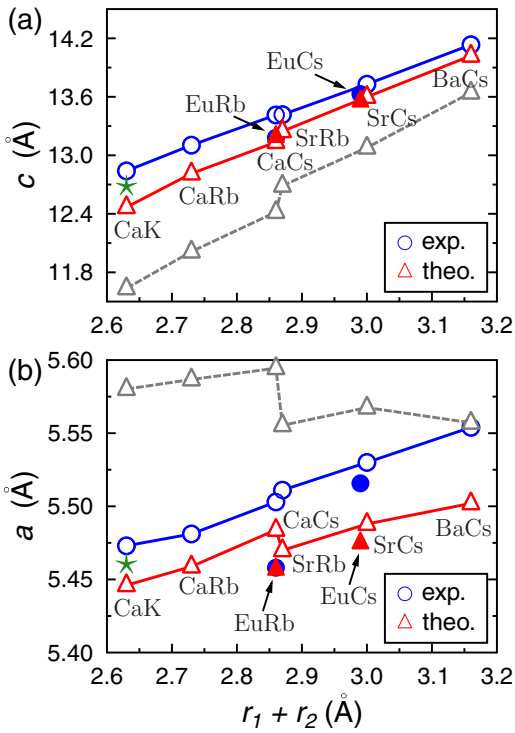

FIG. 3. Correlation between the zero-pressure a- and c-lattice parameters and the sum of the ionic radii $r_1 + r_2$ of the spacer cations (r_1 for Ae and Eu and r_2 for A cations) for different 1144 iron pnictides. The measured (circles) and theoretical values (triangles) are shown for each system. Filled symbols indicate the parameters of the Eu-based systems and the star shows the low-temperature data for $CaKFe_4As_4$ [6]. The theory prediction is obtained using GGA and the spin-vortex configuration of Fe moments, following previous work [4], from which the data for $CaKFe_4As_4$ is taken for this plot. Dashed lines show results of purely nonmagnetic calculations.

deviate by (0.1–0.3) Å from the experimental result, where smaller deviations are observed for compounds with larger spacer cations. One possible source of discrepancy is the fact that the 1144 crystal structures were measured at room temperature [5], while DFT calculations formally correspond to the zero-temperature case, suggesting that thermal expansion can partially explain the observed deviations. For example, the thermal effect in the c parameter of $CaKFe_4As_4$ can be as large as 0.16 Å when going from room temperature down to a few kelvins [6], so that the overall agreement between theory and experiment for this compound is acceptable (compare circles and triangle symbols in Fig. 3).

IV. FIRST HALF-COLLAPSED TETRAGONAL TRANSITION

Assuming a spin-vortex magnetic configuration, we performed pressure simulations for all 1144 materials over a wide range of pressures. The observed evolution of the in-plane, a, and out-of-plane, c, lattice parameters with applied pressure is qualitatively similar in all cases, despite large variations in their absolute values (see Figs. 4 and 5 as well as Figs. 9–13 in Appendix C). At the first hcT transition, the c parameter and the As-As interlayer distances (d_{As-As}) across the cation plane where the c collapse is happening decrease abruptly, while the in-plane parameter a shows an upturn. The As-As $4p_z$ antibonding orbitals lie above the Fermi level as illustrated in Figs. 2(b) and 2(c). As a matter of fact, the As-As distance right after the first hcT is very similar for all 1144 compounds and varies between (2.8–2.9) Å (Table I), which agrees with the chemical nature of cT transitions in these materials.

The estimated critical pressure for the first half-collapsed tetragonal transition (P_{c1} in Table I) shows clear trends as a function of the cation sizes. For all $CaAFe_4As_4$ (A = K, Rb, Cs) systems, the first hcT is observed near 5 GPa, which agrees with the fact that the As-As p_z bonding is happening across the Ca layers in all three systems. When Ae = Ca is replaced by Sr, P_{c1} is shifted to larger values, up to 14–15 GPa for A = Rb and up to 18 GPa for A = Cs. Similar critical pressures for the first hcT are found here for Eu-based 1144 systems, which can be expected based on almost identical ionic radii of Sr and Eu (Table I). The maximal critical pressure P_{c1} of 34 GPa is found for $BaCsFe_4As_4$ with the largest alkaline-earth interlayer cation (Ba). From Table I, it can be observed that for a given Ae cation, increasing the size of the A cation shifts the first hcT phase to higher pressures. Similar to the 122 pnictides, the half-collapsed transitions in the 1144 systems are more

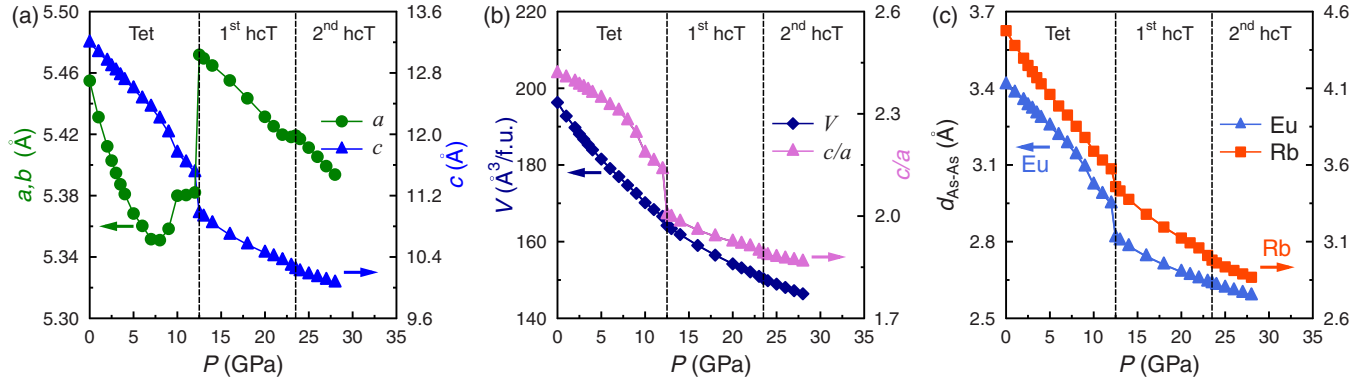

FIG. 4. Pressure evolution of (a) lattice parameters $a = b$ and c, (b) volume and c/a ratio and (c) As-As distances across both hcT transitions for $EuRbFe_4As_4$. The critical pressures of the two half-collapsed transitions are marked by vertical dashed lines. Here, the first hcT and the collapse of Fe moments occur simultaneously.

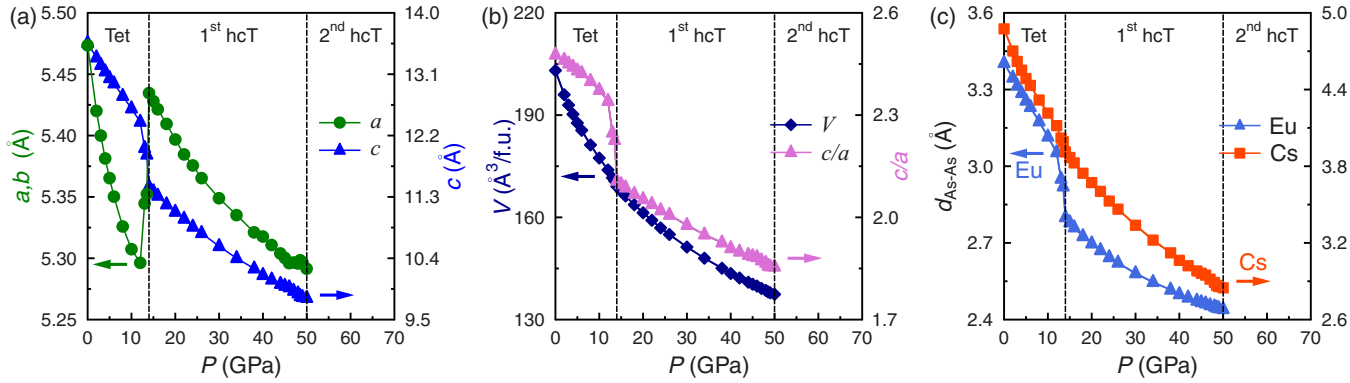

FIG. 5. Pressure evolution of (a) lattice parameters $a = b$ and c, (b) volume and c/a ratio, and (c) As-As distances across both hcT transitions for $EuCsFe_4As_4$. The critical pressures of the two half-collapsed transitions are marked by vertical dashed lines. Here, the first hcT and the collapse of Fe moments occur simultaneously.

abrupt for smaller spacer cations and become broadened for cations with larger ionic radii.

One point to discuss is the consequences of invoking a spin-vortex Fe magnetic order for the structural relaxations under pressure even though these systems at zero pressure do not manifest magnetic order associated with the Fe site. This assumption may lead to slightly overestimated P_{c1}. Whereas we have discussed above the importance of introducing this "frozen" magnetic order, the calculations show, on top of the structural collapse, a "magnetic collapse" that is absent in the real system. Such a collapse may happen simultaneously to the structural collapse or at slightly different pressures as it is the case for $CaRbFe_4As_4$, $CaCsFe_4As_4$, or $BaCsFe_4As_4$ (see the grey area in Figs. 9, 10, and 13). This result may be interpreted in terms of the hcT transition being a broad transition smeared by spin fluctuations.

For the special cases of $EuRbFe_4As_4$ and $EuCsFe_4As_4$ we find the first hcT transition to occur across the Eu layer at a P_{c1} of about 12.5 GPa and 14 GPa, respectively (Figs. 4 and 5). This prediction shows a rather good agreement with the most recent experimental study of pressure effects in $EuRbFe_4As_4$ and $EuCsFe_4As_4$ [13]. In our simulations, Eu magnetism [34] survives well beyond the first hcT transition as has also been recently observed [13]. This indicates that the localized Eu spins are little influenced by the As-As p_z bonding. At much higher pressures, as we discuss below, the second collapse occurs across the Rb plane ($P_{c2} \sim 23.5$ GPa) for $EuRbFe_4As_4$ and across the Cs plane ($P_{c2} \sim 48.5$ GPa) for $EuCsFe_4As_4$. The magnetic order of Eu persists up to the highest studied pressure slightly above the second collapse. No drastic changes of the Eu oxidation state are observed in the whole pressure range. However, from the enthalpy analysis, we observe that the Eu order in $EuRbFe_4As_4$ transforms from FM to AFM near 3 GPa, but gets back to FM at higher pressures. In contrast, $EuCsFe_4As_4$ remains ferromagnetic in the whole pressure range (0–50) GPa, although the energy splitting between the two magnetic states varies significantly in between. These findings motivate a more detailed study including Eu orders with different q vectors, which would clarify the ground state of the *4f*-subsystem in these superconductors.

V. SECOND HALF-COLLAPSED TETRAGONAL TRANSITION

At higher pressures, the studied 1144 systems undergo a second hcT transition in our simulations. In our previous work

TABLE I. Predicted critical pressures P_{c1} and P_{c2} and As-As interlayer distances d_{As-As} for the two hcT transitions in the 1144 series (data for $CaKFe_4As_4$ is taken from Ref. [4]). Note that the values provide indicative trends for the real systems. The ionic radii r_1 and r_2 are provided for the *Ae* and *A* species and Eu [same data in Fig. 1(a)]. The accuracy of the provided critical pressures lies within 0.5 GPa, as determined by the smallest pressure step and convergence of the simulations. Superconducting T_c from Refs. [5,10] is shown for each compound together with the zero-pressure As height asymmetry $\eta_0 = \eta(P = 0)$ defined below by Eq. (1).

			First hcT			Second hcT		
Compound	T_c (K)	η_0 (%)	r_1 (Å)	P_{c1} (GPa)	d_{As-As} (Å)	r_2 (Å)	P_{c2} (GPa)	d_{As-As} (Å)
$CaKFe_4As_4$	33.1	1.47	1.12	4	2.82	1.51	12.4	3.00
$CaRbFe_4As_4$	35.0	1.48	1.12	5.25	2.79	1.61	26	2.95
$CaCsFe_4As_4$	31.6	1.54	1.12	5.8	2.79	1.74	58	2.81
$SrRbFe_4As_4$	35.1	0.76	1.26	14.5	2.88	1.61	24	2.95
$SrCsFe_4As_4$	36.8	0.72	1.26	18	2.78	1.74	46.5	2.88
$BaCsFe_4As_4$	26.0	0.43	1.42	34	2.91	1.74	39	2.97
$EuRbFe_4As_4$	36	0.76	1.25	12.5	2.82	1.61	23.5	2.98
$EuCsFe_4As_4$	35	0.73	1.25	14	2.80	1.74	48.5	2.87

on $CaKFe_4As_4$, we predicted the second structural collapse to occur around 12 GPa [4]. Here, we find that the second critical pressure P_{c2} correlates with the size of the corresponding spacer cation (A = K, Rb, Cs), similar to the first hcT phase, where P_{c1} rapidly increases in the series Ca, Sr, Eu, Ba. The lowest pressure for the second hcT is expected for $CaKFe_4As_4$, whereas the highest one (58 GPa) is found for $CaCsFe_4As_4$. For that reason, the second hcT transition might be difficult to access experimentally.

Interestingly, the second hcT transition has a relatively smaller effect on the lattice parameters (only a small kink is observed for a and c) and is detected in our first-principles calculations again based on the analysis of the As-As $4p_z$ orbital bonding, as demonstrated in Fig. 2. The characteristic As-As distance d_{As-As} across the A layer is around (2.8 – 3.0) Å after the collapse (Table I), which is on average slightly larger than d_{As-As} across the Ae layer at P_{c1}. The smallest critical d_{As-As} of 2.81 Å is found for $CaCsFe_4As_4$, which correlates with the highest critical pressure P_{c2} of 58 GPa. It should be emphasized that, for all studied 1144 systems, the Fe moments are fully suppressed long before the second hcT transition and play no role for this transition. The purely chemical nature of the second half collapse becomes then even more apparent.

VI. As HEIGHT ASYMMETRY

The main difference between the well-known 122 and the new 1144 ($AeAFe_4As_4$) compounds is the broken glide-plane symmetry in the latter case, which creates two types of As sites. This asymmetry of As tetrahedra in the 1144 systems was found to play a leading role for the emergence of spin-vortex magnetism under electron doping [8]. We can characterize this structural property by the parameter

$$\eta = \frac{h(A) - h(Ae)}{h(A) + h(Ae)} \times 100\%, \qquad (1)$$

with $h(Ae)$ and $h(A)$ being the As heights on the side of the Ae and A spacer layers, respectively [Fig. 6(a)].

We find that $h(A)$ is always larger than $h(Ae)$ for all studied 1144 pnictides. Also, the largest As height asymmetry at zero pressure is found for $CaAFe_4As_4$ ($\eta \approx 1.5\%$), while the asymmetry gradually decreases towards 0.4% in the series Ae = Ca, Sr, Ba. As evident from Table I, this fact is directly related to the difference in the ionic radii of the Ae and A cations.

Upon increasing pressure, the As height asymmetry η grows continuously until the first hcT transition is reached where it shows a clear upturn [Fig. 6(b)]. The Fe magnetic collapse in the calculation is always accompanied by a sudden increase of the asymmetry parameter η, while the second hcT transition slightly reduces the asymmetry. These trends are observed for all studied systems.

Since a large As height asymmetry favors the "hedgehog" spin-vortex magnetic order in $CaKFe_4As_4$ [8] and increases under pressure for the studied 1144 systems [example in Fig. 6(b)], we can argue that pressure can stabilize the spin-vortex state relative to the usual stripe phase. On the other hand, $BaCsFe_4As_4$ is predicted here to have a more symmetric As-Fe-As block than other 1144 systems and, for that reason, is likely to be closer to stripe order than the other 1144 compounds.

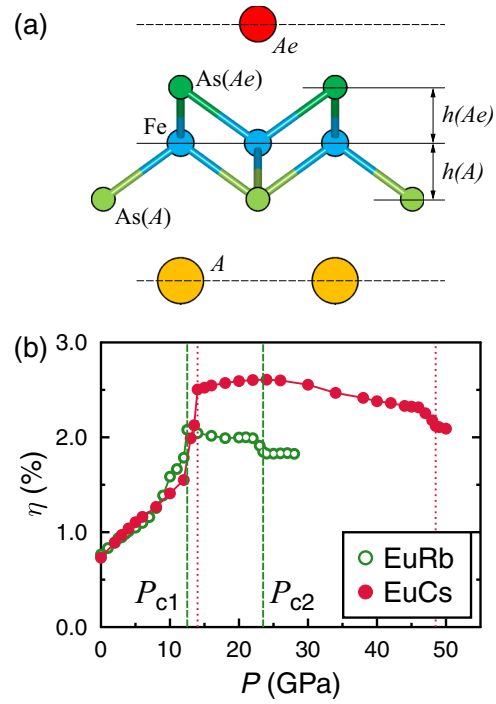

FIG. 6. (a) Definition of two different As heights in 1144 compounds. (b) As height asymmetry Eq. (1) vs pressure for $EuRbFe_4As_4$ and $EuCsFe_4As_4$. The critical pressures P_{c1} and P_{c2} for both hcT are indicated by the vertical dashed (EuRb) and dotted (EuCs) lines. Similar qualitative behavior is observed for other 1144 systems.

VII. CONCLUSION

We performed first-principles DFT simulations under pressure of various members of the 1144 family of Fe-based superconductors and found clear trends in the appearance of layer-selective hcT transitions as well as changes in the electronic properties of these systems. First of all, the critical pressures P_{c1} and P_{c2} for both consecutive hcT transitions increase rapidly with the cation size of the respective spacer layers. This agrees with the already known features of collapse in $AeFe_2As_2$ systems (Ae = Ca, Sr, Ba) [27,32,35–38] and $EuFe_2As_2$ [14,39]. Second, even though the systems considered don't show magnetic long-range order at the Fe sites, it is necessary to include Fe spins in a certain magnetic arrangement in simulations to correctly predict the structure in the low-pressure range. Depending on the chosen chemical composition, the Fe moments either survive or vanish across the structural collapse. In the case of $BaCsFe_4As_4$, the local Fe moments are suppressed even before the formation of As-As bonds.

Based on our calculations, the critical value for the As-As distance leading to a structural collapse varies between (2.8–3.0) Å, depending on the spacer cation size. The initial As-As distance at zero pressure determines then the critical pressure necessary for a structural transition. Finding ways of bringing the 1144 systems closer to the critical As-As separation already at zero pressure will eventually allow the observation of half-collapsed phases at ambient pressure in this class of materials.

For instance, the critical pressures at which the half collapses happen can be significantly reduced in uniaxially compressed systems as has been already observed in 122 systems [27,36,40], making the observation of this structural transition, in principle, possible for some of the explored compounds. Also, study of cT phases in other 1144 systems based on tri- and monovalent spacer cations that were newly suggested to be stable at ambient pressure [41,42], e.g., $LaKFe_4As_4$ and $EuKFe_4As_4$, might be another promising research direction.

For the $EuRbFe_4As_4$ and $EuCsFe_4As_4$ systems, the character of the half-collapsed transition and the critical pressures are similar to the Sr-based systems, which is explained by almost identical ionic radii of Eu and Sr 2+ cations. The Eu magnetism is stable across both collapse transitions, with the *4f* moments staying close to the expected value of 7 μ_B. Very recent experimental observations [13] seem to confirm the predicted pressure trends. In addition, our simulations suggest that the ordering vector of Eu may change under pressure in the $EuRbFe_4As_4$ system.

In view of the novel magnetism discovered recently in electron-doped $CaKFe_4As_4$ [8], the rest of the 1144 family is worth studying in terms of their magnetic properties. $CaRbFe_4As_4$ and $CaCsFe_4As_4$ have the largest As height asymmetry and are therefore promising candidates for a spin-vortex magnetic crystal with a high ordering temperature. Search for other 1144 materials with a larger difference in the two cation sizes, leading to a stronger asymmetry between the As sites, appears to be a natural next step. In contrast, 1144 systems with bigger cations, such as $BaCsFe_4As_4$, have a more symmetric structure and are likely to be closer to stripe order than more asymmetric 1144 compounds. The motivation to look for further spin-vortex ordered Fe-based systems is the recently proposed relation of this magnetic order to the strong unconventional superconductivity in 1144 systems. Furthermore, this is a unique example of a noncollinear double-Q magnetic order in iron pnictides and presents an important part of their general phase diagram [8].

ACKNOWLEDGMENTS

This work was financially supported by DFG Sonderforschungsbereich TRR 49. Work at Ames Lab (P.C.C.) was supported by the U.S. Department of Energy, Office of Basic Energy Science, Division of Materials Sciences and Engineering. Ames Laboratory is operated for the U.S. Department of Energy by Iowa State University under Contract No. DE-AC02-07CH11358. Research (V.B.) was funded in part by the Gordon and Betty Moore Foundation's EPiQS Initiative through Grant No. GBMF4411. This work was initiated as part of the Humboldt Prize for P.C.C. The computer time was allotted by the center for supercomputing (CSC) in Frankfurt and by the computer center of Goethe University. V.B. and R.V. acknowledge discussions with Peter Hirschfeld and James Hamlin. Parts of some figures have been produced with VESTA3 [43].

APPENDIX A: ROLE OF LOCAL Fe MOMENTS

As emphasized in the main text, the presence of local Fe moments is a necessary ingredient of our simulations, since otherwise the predicted structures would have a largely underestimated c-lattice parameter, which, in case of $CaRbFe_4As_4$, even leads to the formation of As-As bonds near Ca already at zero pressure, confirmed by the band structure analysis (Fig. 7). We have also performed some test calculations with Fe magnetic orders other than spin vortex and found that the best agreement with structural parameters from experiment is achieved assuming a spin-vortex arrangement of Fe moments.

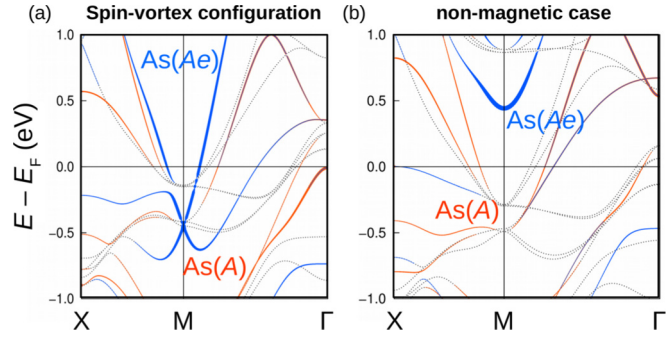

FIG. 7. Comparison of the As-4p_z orbitals for $CaRbFe_4As_4$ structures relaxed at zero pressure (a) using the spin-vortex Fe order or (b) nonmagnetically. In the latter case, the As-As bonds across Ca are already formed, as opposed to the former structure, which emphasizes the importance of spin-vortex fluctuations in 1144 systems. For both relaxed geometries, the band structure is non-spin-polarized [31]. The color code is the same as in Fig. 2.

APPENDIX B: ACCURACY OF STRUCTURE OPTIMIZATION

Regarding the accuracy of our pressure simulations, as mentioned in the main text and illustrated in Fig. 8, the increase of the energy cutoff from 600 eV to 800 eV leads to rather small changes in the lattice parameters, which do not affect the general trends in the 1144 family.

APPENDIX C: STRUCTURE-EVOLUTION UNDER PRESSURE

The pressure-dependence of the in-plane (a) and out-of-plane (c) lattice parameters along with the As-As distances

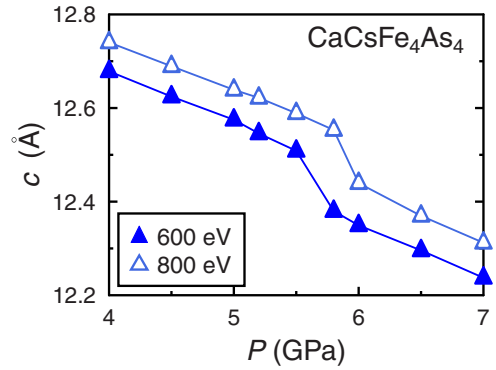

FIG. 8. Comparison of the calculated pressure-dependent c-lattice parameter of $CaCsFe_4As_4$ for two different energy cutoff values 600 eV and 800 eV.

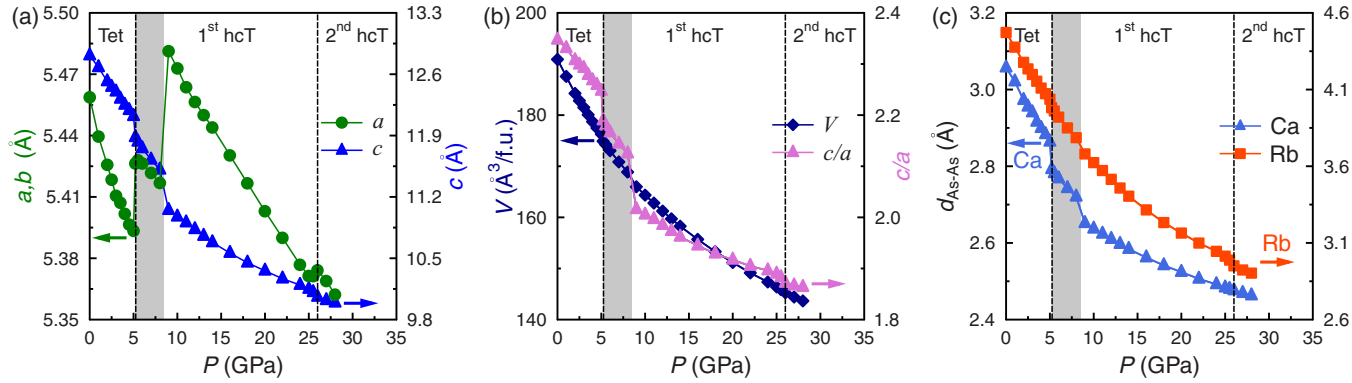

FIG. 9. Pressure evolution of (a) lattice parameters $a = b$ and c, (b) volume and c/a ratio, and (c) As-As distances across both hcT transitions for $CaRbFe_4As_4$. The critical pressures of the two half-collapsed transitions are marked by vertical dashed lines and the pressure range between the first hcT and the subsequent collapse of Fe moments is indicated by shading.

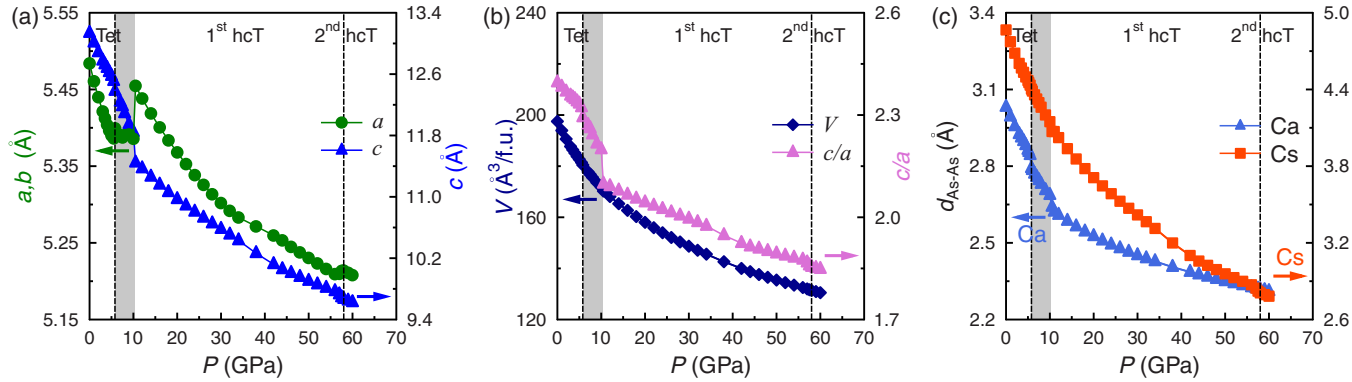

FIG. 10. Pressure evolution of (a) lattice parameters $a = b$ and c, (b) volume and c/a ratio, and (c) As-As distances across both hcT transitions for $CaCsFe_4As_4$. The critical pressures of the two half-collapsed transitions are marked by vertical dashed lines and the pressure range between the first hcT and the subsequent collapse of Fe moments is indicated by shading.

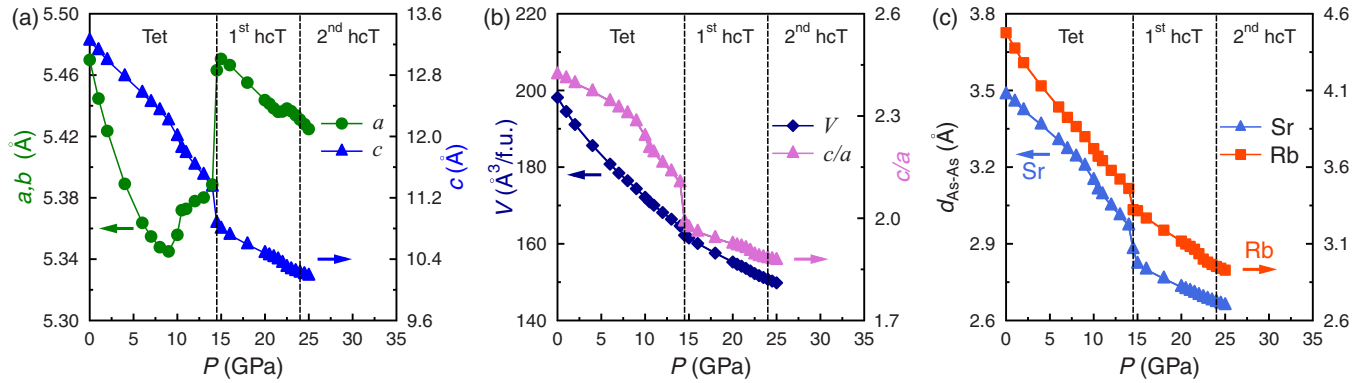

FIG. 11. Pressure evolution of (a) lattice parameters $a = b$ and c, (b) volume and c/a ratio, and (c) As-As distances across both hcT transitions for $SrRbFe_4As_4$. The critical pressures of the two half-collapsed transitions are marked by vertical dashed lines. Here, the first hcT and the collapse of Fe moments occur simultaneously.

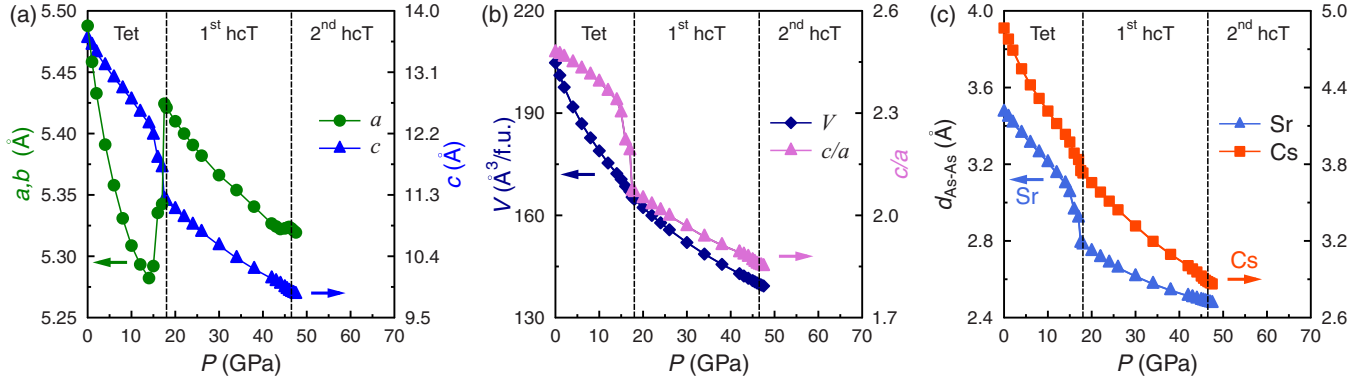

FIG. 12. Pressure evolution of (a) lattice parameters $a = b$ and c, (b) volume and c/a ratio, and (c) As-As distances across both hcT transitions for $SrCsFe_4As_4$. The critical pressures of the two half-collapsed transitions are marked by vertical dashed lines. Here, the first hcT and the collapse of Fe moments occur simultaneously.

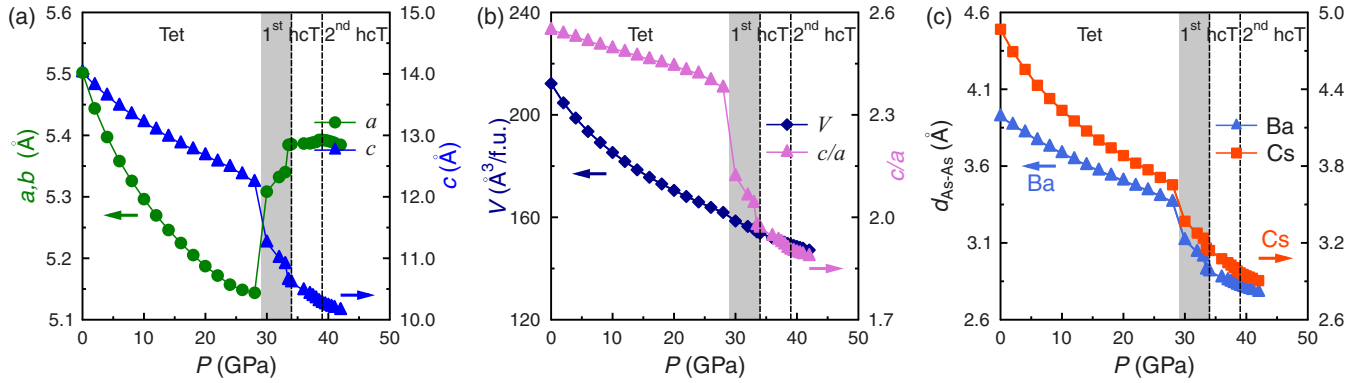

FIG. 13. Pressure evolution of (a) lattice parameters $a = b$ and c, (b) volume and c/a ratio, and (c) As-As distances across both hcT transitions for $BaCsFe_4As_4$. The critical pressures of the two half-collapsed transitions are marked by vertical dashed lines and the pressure range between the collapse of Fe moments and the subsequent first hcT is indicated by shading.

across both collapse transitions is summarized for all studied 1144 systems in Figs. 4, 5, and 9–13. At the first half collapse, the qualitative behavior is the same for all $CaAFe_4As_4$ compounds, but for $SrRbFe_4As_4$ and $SrCsFe_4As_4$ the structural collapse transition overlaps with the suppression of Fe moments. $BaCsFe_4As_4$ seems to be an extreme case, since it shows the magnetic collapse first and then undergoes an actual half collapse at a somewhat higher pressure.

[1] A. Kreyssig, M. A. Green, Y. Lee, G. D. Samolyuk, P. Zajdel, J. W. Lynn, S. L. Bud'ko, M. S. Torikachvili, N. Ni, S. Nandi, J. B. Leão, S. J. Poulton, D. N. Argyriou, B. N. Harmon, R. J. McQueeney, P. C. Canfield, and A. I. Goldman, Pressure-induced volume-collapsed tetragonal phase of $CaFe_2As_2$ as seen via neutron scattering, Phys. Rev. B **78**, 184517 (2008).

[2] P. C. Canfield and S. L. Bud'ko, FeAs-based superconductivity: A case study of the effects of transition metal doping on $BaFe_2As_2$, Annu. Rev. Condens. Matter Phys. **1**, 27 (2010).

[3] T. Yildirim, Strong Coupling of the Fe-Spin State and the As-As Hybridization in Iron-Pnictide Superconductors from First-Principle Calculations, Phys. Rev. Lett. **102**, 037003 (2009).

[4] U. S. Kaluarachchi, V. Taufour, A. Sapkota, V. Borisov, T. Kong, W. R. Meier, K. Kothapalli, B. G. Ueland, A. Kreyssig, R. Valentí, R. J. McQueeney, A. I. Goldman, S. L. Bud'ko, and P. C. Canfield, Pressure-induced half-collapsed-tetragonal phase in $CaKFe_4As_4$, Phys. Rev. B **96**, 140501(R) (2017).

[5] A. Iyo, K. Kawashima, T. Kinjo, T. Nishio, S. Ishida, H. Fujihisa, Y. Gotoh, K. Kihou, H. Eisaki, and Y. Yoshida, New-structure-type Fe-based superconductors: $CaAFe_4As_4$ (A = K, Rb, Cs) and $SrAFe_4As_4$ (A = Rb, Cs), J. Am. Chem. Soc. **138**(10), 3410 (2016).

[6] W. R. Meier, T. Kong, U. S. Kaluarachchi, V. Taufour, N. H. Jo, G. Drachuck, A. E. Böhmer, S. M. Saunders, A. Sapkota, A. Kreyssig, M. A. Tanatar, R. Prozorov, A. I. Goldman, F. F. Balakirev, A. Gurevich, S. L. Bud'ko, and P. C. Canfield, Anisotropic thermodynamic and transport properties of single-crystalline $CaKFe_4As_4$, Phys. Rev. B **94**, 064501 (2016).

[7] S. L. Bud'ko, T. Kong, W. R. Meier, X. Ma, and P. C. Canfield, ^{57}Fe Mössbauer study of stoichiometric iron-based superconductor $CaKFe_4As_4$: A comparison to KFe_2As_2 and $CaFe_2As_2$, Philos. Mag. **97**, 2689 (2017).

[8] W. R. Meier, Q.-P.Ding, A. Kreyssig, S. L. Bud'ko, A. Sapkota, K. Kothapalli, V. Borisov, R. Valentí, C. D. Batista, P. P. Orth,

R. M. Fernandes, A. I. Goldman, Y. Furukawa, A. E. Böhmer, and P. C. Canfield, Hedgehog spin-vortex crystal stabilized in a hole-doped iron-based superconductor, npj Quantum Mater. **3**, 5 (2018).

[9] R. D. Shannon, Revised effective ionic radii and systematic studies of interatomic distances in halides and chalcogenides, Acta Cryst. A **32**, 751 (1976).

[10] K. Kawashima, T. Kinjo, T. Nishio, S. Ishida, H. Fujihisa, Y. Gotoh, K. Kihou, H. Eisaki, Y. Yoshida, and A. Iyo, Superconductivity in Fe-based compound EuAFe$_4$As$_4$ (A = Rb and Cs), J. Phys. Soc. Jpn. **85**, 064710 (2016).

[11] Y. Liu, Y.-B. Liu, Q. Chen, Z.-T. Tang, W.-H. Jiao, Q. Tao, Z.-A. Xu, and G.-H. Cao, A new ferromagnetic superconductor: CsEuFe$_4$As$_4$, Sci. Bull. **61**, 1213 (2016).

[12] Y. Liu, Y.-B. Liu, Y.-L. Yu, Q. Tao, C.-M. Feng, and G.-H. Cao, RbEu(Fe$_{1-x}$Ni$_x$)$_4$As$_4$: From a ferromagnetic superconductor to a superconducting ferromagnet, Phys. Rev. B **96**, 224510 (2017).

[13] D. E. Jackson, D. VanGennep, W. Bi, D. Zhang, P. Materne, Y. Liu, G.-H. Cao, S. T. Weir, Y. K. Vohra, and J. J. Hamlin, Superconducting and magnetic phase diagram of RbEuFe$_4$As$_4$ and CsEuFe$_4$As$_4$ at high pressure, Phys. Rev. B **98**, 014518 (2018).

[14] S. Zapf and M. Dressel, Europium-based iron pnictides: a unique laboratory for magnetism, superconductivity and structural effects, Rep. Prog. Phys. **80**, 016501 (2017).

[15] J. T. Sypek, H. Yu, K. J. Dusoe, G. Drachuck, H. Patel, A. M. Giroux, A. I. Goldman, A. Kreyssig, P. C. Canfield, S. L. Bud'ko, C. R. Weinberger, and S.-W. Lee, Superelasticity and cryogenic linear shape memory effects of CaFe$_2$As$_2$, Nat. Commun. **8**, 1083 (2017).

[16] P. E. Blöchl, Projector augmented-wave method, Phys. Rev. B **50**, 17953 (1994).

[17] G. Kresse and D. Joubert, From ultrasoft pseudopotentials to the projector augmented-wave method, Phys. Rev. B **59**, 1758 (1999).

[18] G. Kresse and J. Hafner, *Ab initio* molecular dynamics for liquid metals, Phys. Rev. B (Rapid Commun.) **47**, 558 (1993).

[19] G. Kresse and J. Furthmüller, Efficient iterative schemes for *ab initio* total-energy calculations using a plane-wave basis set, Phys. Rev. B **54**, 11169 (1996).

[20] G. Kresse and J. Furthmüller, Efficiency of ab-initio total energy calculations for metals and semiconductors using a plane-wave basis set, Comput. Mater. Sci. **6**, 15 (1996).

[21] J. P. Perdew, K. Burke, and M. Ernzerhof, Generalized Gradient Approximation Made Simple, Phys. Rev. Lett. **77**, 3865 (1996).

[22] S. L. Dudarev, G. A. Botton, S. Y. Savrasov, C. J. Humphreys, and A. P. Sutton, Electron-energy-loss spectra and the structural stability of nickel oxide: An LSDA+U study, Phys. Rev. B **57**, 1505 (1998).

[23] A. I. Liechtenstein, V. I. Anisimov, and J. Zaanen, Density-functional theory and strong interactions: Orbital ordering in Mott-Hubbard insulators, Phys. Rev. B **52**, R5467(R) (1995).

[24] J. Cui, Q.-P. Ding, W. R. Meier, A. E. Böhmer, T. Kong, V. Borisov, Y. Lee, S. L. Bud'ko, R. Valentí, P. C. Canfield, and Y. Furukawa, Magnetic fluctuations and superconducting properties of CaKFe$_4$As$_4$ studied by ^{75}As NMR, Phys. Rev. B **96**, 104512 (2017).

[25] Y.-Z. Zhang, H. C. Kandpal, I. Opahle, H. O. Jeschke, and R. Valentí, Microscopic origin of pressure-induced phase transitions in the iron pnictide superconductors AFe$_2$As$_2$: An ab initio molecular dynamics study, Phys. Rev. B **80**, 094530 (2009).

[26] N. Colonna, G. Profeta, A. Continenza, and S. Massidda, Structural and magnetic properties of CaFe$_2$As$_2$ and BaFe$_2$As$_2$ from first-principles density functional theory, Phys. Rev. B **83**, 094529 (2011).

[27] M. Tomić, R. Valentí, and H. O. Jeschke, Uniaxial versus hydrostatic pressure-induced phase transitions in CaFe$_2$As$_2$ and BaFe$_2$As$_2$, Phys. Rev. B **85**, 094105 (2012).

[28] R. S. Dhaka, R. Jiang, S. Ran, S. L. Bud'ko, P. C. Canfield, B. N. Harmon, A. Kaminski, M. Tomić, R. Valentí, and Y. Lee, Dramatic changes in the electronic structure upon transition to the collapsed tetragonal phase in CaFe$_2$As$_2$, Phys. Rev. B **89**, 020511 (2014).

[29] S. L. Bud'ko, X. Ma, M. Tomić, S. Ran, R. Valentí, and P. C. Canfield, Transition to collapsed tetragonal phase in CaFe$_2$As$_2$ single crystals as seen by ^{57}Fe Mössbauer spectroscopy, Phys. Rev. B **93**, 024516 (2016).

[30] K. Koepernik and H. Eschrig, Full-potential nonorthogonal local-orbital minimum-basis band-structure scheme, Phys. Rev. B **59**, 1743 (1999).

[31] Although it is absolutely necessary to include Fe magnetic order in the structural optimization, the subsequent analysis of As orbitals relevant to the half-collapsed tetragonal transition can be successfully done based on a nonmagnetic band structure, since the As sites are barely spin-polarized by the neighboring Fe moments. The only exceptions are EuRbFe$_4$As$_4$ and EuCsFe$_4$As$_4$ systems, where As orbitals acquire a moderate spin splitting due to the ferromagnetically ordered Eu sites.

[32] D. Kasinathan, M. Schmitt, K. Koepernik, A. Ormeci, K. Meier, U. Schwarz, M. Hanfland, C. Geibel, Y. Grin, A. Leithe-Jasper, and H. Rosner, Symmetry-preserving lattice collapse in tetragonal SrFe$_{2-x}$Ru$_x$As$_2$ (x = 0, 0.2): A combined experimental and theoretical study, Phys. Rev. B **84**, 054509 (2011).

[33] J. Diehl, S. Backes, D. Guterding, H. O. Jeschke, and R. Valentí, Correlation effects in the tetragonal and collapsed-tetragonal phase of CaFe$_2$As$_2$, Phys. Rev. B **90**, 085110 (2014).

[34] Please note that in our simulations we didn't consider more complex cases of Eu magnetism than ferromagnetism and stripelike antiferromagnetism.

[35] R. Mittal, S. K. Mishra, S. L. Chaplot, S. V. Ovsyannikov, E. Greenberg, D. M. Trots, L. Dubrovinsky, Y. Su, T. Brueckel, S. Matsuishi, H. Hosono, and G. Garbarino, Ambient- and low-temperature synchrotron x-ray diffraction study of BaFe$_2$As$_2$ and CaFe$_2$As$_2$ at high pressures up to 56 GPa, Phys. Rev. B **83**, 054503 (2011).

[36] M. Tomić, H. O. Jeschke, R. M. Fernandes, and R. Valentí, In-plane uniaxial stress effects on the structural and electronic properties of BaFe$_2$As$_2$ and CaFe$_2$As$_2$, Phys. Rev. B **87**, 174503 (2013).

[37] D. Guterding, S. Backes, M. Tomić, H. O. Jeschke, and R. Valentí, Ab initio perspective on structural and electronic properties of iron-based superconductors, Phys. Status Solidi (b) **254**, 1600164 (2016).

[38] C. Tresca and G. Profeta, Compressed tetragonal phase in XFe$_2$As$_2$ (X = Na, K, Rb, Cs) and in the alloy Na$_{0.5}$K$_{0.5}$Fe$_2$As$_2$, Phys. Rev. B **95**, 165129 (2017).

[39] W. Uhoya, G. Tsoi, Y. K. Vohra, M. A. McGuire, A. S. Sefat, B. C. Sales, D. Mandru, and S. T. Weir, Anomalous compressibility effects and superconductivity of $EuFe_2As_2$ under high pressures, J. Phys.: Condens. Matter **22**, 292202 (2010).

[40] K. Prokeš, A. Kreyssig, B. Ouladdiaf, D. K. Pratt, N. Ni, S. L. Bud'ko, P. C. Canfield, R. J. McQueeney, D. N. Argyriou, and A. I. Goldman, Evidence from neutron diffraction for superconductivity in the stabilized tetragonal phase of $CaFe_2As_2$ under uniaxial pressure, Phys. Rev. B **81**, 180506 (2010).

[41] B. Q. Song, M. C. Nguyen, C. Z. Wang, P. C. Canfield, and K. M. Ho, Whether it is possible to stabilize the 1144-phase pnictides with tri-valence cations? arXiv:1710.01868v2.

[42] B. Q. Song, M. C. Nguyen, C. Z. Wang, and K. M. Ho, Stability of the 1144 phase in iron pnictides, Phys. Rev. B **97**, 094105 (2018).

[43] K. Momma and F. Izumi, VESTA3 for three-dimensional visualization of crystal, volumetric and morphology data, J. Appl. Cryst. **44**, 1272 (2011).